A Multimodal Assessment of Melanin and Melanocyte Activity in Abnormally Pigmented Hypertrophic Scar

Taryn E. Travis, MD,* Pejhman Ghassemi, PhD,† Jessica C. Ramella-Roman, PhD,‡ Nicholas J. Prindeze, BSc,* Dereck W. Paul, BSc,* Lauren T. Moffatt, PhD,* Marion H. Jordan, MD, FACS,* Jeffrey W. Shupp, MD*†

Using a validated swine model of human scar formation, hyperpigmented and hypopigmented scar samples were examined for their histological and optical properties to help elucidate the mechanisms and characteristics of dyspigmentation. Full-thickness wounds were created on the flanks of red Duroc pigs and allowed to heal. Biopsies from areas of hyperpigmentation, hypopigmentation, and uninjured tissue were fixed and embedded for histological examination using Azure B and primary antibodies to S100B, HMB45, and α-melanocyte-stimulating hormone (α-MSH). Spatial frequency domain imaging (SFDI) was then used to examine the optical properties of scars. Hyperpigmentation was first noticeable in healing wounds around weeks 2 to 3, gradually becoming darker. There was no significant difference in S100B staining for the presence of melanocytes between hyperpigmented and hypopigmented scar samples. Azure B staining of melanin was significantly greater in histological sections from hyperpigmented areas than in sections from both uninjured skin and hypopigmented scar ($P < .0001$). There was significantly greater staining for α-MSH in hyperpigmented samples compared with hypopigmented samples ($P = .0121$), and HMB45 staining was positive for melanocytes in hyperpigmented scar. SFDI at a wavelength of 632 nm resulted in an absorption coefficient map correlating with visibly hyperpigmented areas of scars. In a red Duroc model of hypertrophic scar formation, melanocyte number is similar in hyperpigmented and hypopigmented tissues. Hyperpigmented tissues, however, show a greater amount of melanin and α-MSH, along with immunohistochemical evidence of stimulated melanocytes. These observations encourage further investigation of melanocyte stimulation and the inflammatory environment within a wound that may influence melanocyte activity. Additionally, SFDI can be used to identify areas of melanin content in mature, pigmented scars, which may lead to its usefulness in wounds at earlier time points before markedly apparent pigmentation abnormalities. (J Burn Care Res 2015;36:77–86)

Abnormal pigmentation in scars presents a challenge to clinicians and can be a source of distress to many patients.[1] These types of scars are common after cutaneous trauma and are especially prevalent and psychosocially impactful in individuals recovering from burn injury.[2,3] Although normal skin pigmentation is fairly well understood,[4] the mechanisms that lead to both hypopigmentation and hyperpigmentation in scars are less clear.[5] In order to target and improve abnormal pigmentation as a sequela of burn injury, its role in hypertrophic scar must be better understood.

It is generally accepted that baseline skin pigmentation as well as sun tanning are not a function of melanocyte quantity, but rather a function of the activity of these melanocytes, either in the ratio of eumelanin (brown-black) to pheomelanin (red-yellow) or in the amount of melanin an activated melanocyte produces. Histologically, melanocytes appear as fusiform dendritic cells located in the basal layer of the epidermis,

*From the *Burn Center, Department of Surgery, MedStar Washington Hospital Center, MedStar Health Research Institute; †Department of Biomedical Engineering, Catholic University of America, Washington, District of Columbia; and ‡Department of Biomedical Engineering, Florida International University, Miami.*

Supported by the National Institutes of Health R15EB013439 and The DC Firefighters' Burn Foundation.

Address correspondence to Jeffrey W. Shupp, MD, The Burn Center, 110 Irving Street, NW, Suite 3B-55, Washington, District of Columbia 20010.

1559-047X/2015

DOI: 10.1097/BCR.0000000000000154

and one melanocyte is typically associated with 30 to 40 keratinocytes.[6,7] Melanosomes, or melanin-containing granules, are exported from melanocytes to nearby keratinocytes, leading to visible pigment. Once melanosomes have entered keratinocytes, they are normally distributed toward the superficial side of the nucleus to shield it from ultraviolet radiation.[4] Differences in the quantity, content, and distribution of these melanosomes lead to differences in pigmentation, whereas pure numbers of melanocytes are less variable between individuals. The abnormal behavior of melanocytes has largely been studied with respect to melanoma, and their behavior in the dyspigmentation of scars is still inadequately understood.

Melanocytes and their secretion products have been associated with components of different fibroproliferative processes. Areas of the human body more prone to keloid formation have been found to have higher melanocyte concentrations, while in vitro studies have shown that fibroblasts in coculture with melanocytes proliferate more quickly than those without melanocytes, exhibiting increased mRNA expression levels for type I collagen and transforming growth factor-β1 (TGF-β1).[8] α-Melanocyte-stimulating hormone (α-MSH), a key component of melanogenesis, has been shown to be present in the migrating epithelial edge and wound bed of early full-thickness excisional murine wounds, as well as in the sebaceous glands and epidermis of uninjured tissue adjacent to wounds.[9] In human burn wounds, α-MSH is present in dermal fibroblasts and epidermal keratinocytes early in the healing process, and later can be identified in dermal fibroblasts and epidermal keratinocytes of hypertrophic scar.[9]

Duroc swine are known to scar with varying degrees of abnormal pigmentation, but prior to injury possess uniformly colored red-brown to brown-black skin and provide an excellent model for human wound healing.[10–12] In the current study, characteristics of hypopigmented and hyperpigmented scar as well as the optical properties of melanin were investigated in a validated model of hypertrophic scar. The primary aim was to evaluate whether quantifiable differences exist in factors hypothesized to result in abnormal pigmentation in hyperpigmented and hypopigmented scar. To this end, melanocyte quantity, melanocyte activation, melanin content, and α-MSH were examined.

METHODS

Animal Model and Wound Creation

All animal work described was reviewed and approved by the MedStar Health Research Institute's Institutional Animal Care and Use Committee. Juvenile castrated male Duroc swine (30–55 kg) were received and handled according to facility standard operating procedures under an animal care and use program accredited by the Association for Assessment and Accreditation of Laboratory Animal Care International and Public Health Service Animal Welfare.

On the day of surgery, animals were anesthetized with a combination of ketamine and xylazine that were delivered intramuscularly. Animals were intubated, maintained on isoflurane, placed on a warming blanket, and ventilated while heart rate, blood pressure, peripheral oxygen saturation, end-tidal carbon dioxide saturation, and core body temperature were continuously monitored by trained research staff. The body hair was clipped and the skin was prepped with chlorhexidine gluconate scrub. To create full-thickness wounds, one 4 inch × 4 inch (10.16 cm × 10.16 cm) square was excised over the rib cage on each side of the animal, at a total depth of 0.090 inches (0.030 inch × 3 passes) using a Zimmer dermatome (Zimmer, Ltd., Swindon, UK). In previous experience, this wound creation technique consistently results in hypertrophic scars.[13] Punch biopsies (3 mm) were taken at baseline (preexcision) and immediately postexcision and placed in formalin for subsequent histology. Mepilex® Ag dressings (Monlylke, Gothenburg, Sweden) were applied to wounds after wound creation and at each dressing change. Animals were fitted with custom-made 2 to 3-mm-thick neoprene vests,[14] which completely covered the applied dressings while allowing mobility of the animal. Buprenorphine and fentanyl were administered for pain control at the end of each surgical procedure. Animals returned to the operating room every 7 days until day 133 postwound creation for examinations, imaging, dressing changes, and biopsies. The animals were examined at least twice daily to monitor animal health and to identify any signs of pain, wound infection, or distress.

Spectral Imaging

The spatial frequency domain imaging (SFDI) module of a spectropolarimetric system previously described[15–17] was used to image the absorption and scattering coefficients of reepithelialized scars at the described weekly time points, beginning at reepithelialization of wounds. Images were subsequently processed to develop optical properties calculations that were related to pathophysiology of the scar tissue. Briefly, wound optical properties μ_a and μ_s at different wavelengths are obtained, as well as the rough surface signature as a function of the incident

illumination angle. From the total μ_a, the concentrations of melanin (M), total hemoglobin (V_{blood}), and water (W) are calculated using a minimization algorithm, Equation 1, and tabulated values of oxygenated and deoxygenated hemoglobin (μ_{a_oxy} and μ_{a_deoxy}), water (μ_{a_water}), and melanin ($\mu_{a\_melanin}$) at the selected wavelengths.[18,19]

$$\mu_{a\_tot} = V_{blood}(S\mu_{a\_oxy} + (1-S)\mu_{a\_deoxy}) + W\mu_{a\_water} + M\mu_{a\_melanin} \quad (1)$$

Therefore, the minimization algorithm in combination with tabulated data of melanin, oxygenated and deoxygenated hemoglobin, and water absorption coefficient were used to reconstruct maps of melanin volume fraction. Ultimately this information was used to quantify abnormal melanin concentration in normal skin, hypopigmented scar, and hyperpigmented scar.

Histology

Punch biopsies taken from areas of hyperpigmentation and hypopigmentation were fixed in 10% formalin and embedded in paraffin. Paraffin blocks were sectioned at a thickness of 5 μm and baked at 60°C. After cooling, slides were deparaffinized and rehydrated with phosphate-buffered saline (PBS). Antigen retrieval was performed in Tris-EDTA buffer at 95 to 100°C for 20 minutes. Slides were then cooled for 5 minutes in running cold water. Slides were washed in 0.025% Triton X-100 for 5 minutes two times. Slides were blocked in 5% nonfat milk and 1% BSA, in PBS for 1 hour. After blocking, slides were incubated with monoclonal mouse anti-S100 beta (Abcam, Cambridge, UK), polyclonal rabbit anti-α-MSH (Thermo Fisher Scientific Inc., Waltham, MA), or monoclonal mouse anti-HMB45 (Abcam) primary antibody diluted in PBS 0.05% Tween-20 at 4°C overnight. Negative control slides were incubated with PBS–Tween 20 only. After overnight incubation with primary antibody, slides were rinsed with 0.025% Triton-X-100 for 5 minutes two times, then treated according to methods described for immunofluorescent immunohistochemistry or immunohistochemistry with Azure B staining.

Following the above methods for histology, polyclonal goat anti-mouse immunoglobulin G-Florescein isothiocyanate conjugated (EMD Millipore, Billerica, MA) or polyclonal goat anti-rabbit IgG-CY3 conjugated (Abcam) secondary antibody diluted in PBS 0.05% Tween-20 was applied for 1 hour at room temperature. Slides were rinsed with PBS for 5 minutes three times, then counterstained with 4',6-diamino-2-phenylindole (DAPI; Santa Cruz Biotechnology, Dallas, TX) for 10 minutes. Slides were then viewed with a Zeiss Axioimager microscope and multichannel black and white camera equipped with fluorescence filters (Carl Zeiss, Oberkochen, Germany).

Following the above methods for histology, endogenous peroxidase activity was quenched with 15-minute incubation in 0.3% H_2O_2. Goat polyclonal anti-mouse IgG+IgM-HRP (Abcam) secondary antibody diluted in PBS 0.05% Tween-20 was applied for 2 hours at room temperature. Slides were rinsed with PBS for 5 minutes three times, then developed with 3,3'-diaminobenzidine (DAB) peroxidase substrate (Vector Laboratories, Burlingame, CA) for 10 minutes. After a 5-minute rinse with running tap water, slides were stained with Azure B (Sigma-Aldrich, St. Louis, MO) for 30 minutes, then rinsed in running tap water. Lastly, slides were counterstained with hematoxylin, cleared, and mounted, then viewed with a Zeiss Axioimager microscope and brightfield color camera (Carl Zeiss).

Image Analysis

Hyperpigmented and hypopigmented scar samples for all time points after the appearance of pigmentation were stained and imaged in duplicate. Immunofluorescent images stained for S100B were examined at ×400 magnification, and after the confirmation of a lack of staining in negative controls, the number of positively stained cells per ×400 field was manually counted and recorded. Immunofluorescent images stained for α-MSH were examined at ×100 magnification, and after the recording of background CY3 staining levels in negative control images, positively stained images were analyzed for CY3 expression levels using Zeiss Zen software (Carl Zeiss). Control background staining levels were subtracted from CY3 levels of positively stained slides, then CY3 expression levels were calculated normalized to DAPI expression. Azure B and HMB45/DAB stained images were examined at ×400 magnification, and after the confirmation of a lack of staining in negative controls, Azure-B-stained melanin was quantified as a percentage of the imaged area using Image J software (available from the National Institutes of Health) with a blue image stack threshold set at 160. HMB45-positively stained cells were manually counted per ×400 viewing field. All image analysis data were checked for outliers with Grubbs' test with an α set at 0.05. Averages, SDs, and statistical significance with a two-tailed, unpaired *t*-test were calculated. Statistical significance was set at $P < .05$. Prism GraphPad Software (GraphPad Software, Inc., La Jolla, CA) was used for graphical representations of results.

RESULTS

Peripheral hyperpigmentation directly adjacent to normal uninjured skin began to appear as early as day 14 after injury (Figure 1B, arrowhead). Early after the completion of epithelialization, peripheral hyperpigmentation continued to increase in area and darkness of color, with the additional appearance of an island of hyperpigmentation surrounded by erythematous, hypopigmented skin (Figure 1C). A firm, hypertrophic scar is usually apparent in this model by day 70,[13] with fading erythema and increasing areas of peripheral hyperpigmentation. Additionally, a new island of hyperpigmentation surrounded by hypopigmented tissue appeared around day 70 in the animal pictured in Figure 1D. Figure 1E depicts day 91 after wound creation, with continued firm hypertrophic scar and largely resolved erythema. Additionally, the central island of hyperpigmentation is shown merged with the superior periphery of hyperpigmentation, and the newer area of hyperpigmentation first noticeable at day 70 has greatly increased in size and darkness of color. Day 126, or week 18, after wound healing is shown in Figure 1F, with continued increases in hyperpigmentation, but the maintenance of a border of hypopigmented scar surrounding the hyperpigmented island seen in the left lower corner. The areas of hyperpigmentation generally increased in size and pigmentation over time, with peripheral hyperpigmentation showing the appearance of pigment migration or spread toward the center of the wound/scar (Figure 2A). Additionally, while some islands of hyperpigmented tissue not associated with uninjured skin or hair follicles eventually merged with peripheral areas of hyperpigmentation, as shown in Figure 1E, others remained surrounded by hypopigmented scar for the duration of the 133-day observation period (Figures 1D–F and 2B). Erythema in hypopigmented scar faded with time, but interestingly these areas remained substantially lighter in color than the surrounding uninjured skin or baseline uninjured skin (Figure 1).

During the period of scar observation, regions of interest were imaged with the SFDI module of a spectropolarimetric system.[15–17] Reference sutures were used to recreate the same imaging region of interest from week to week, which can be seen

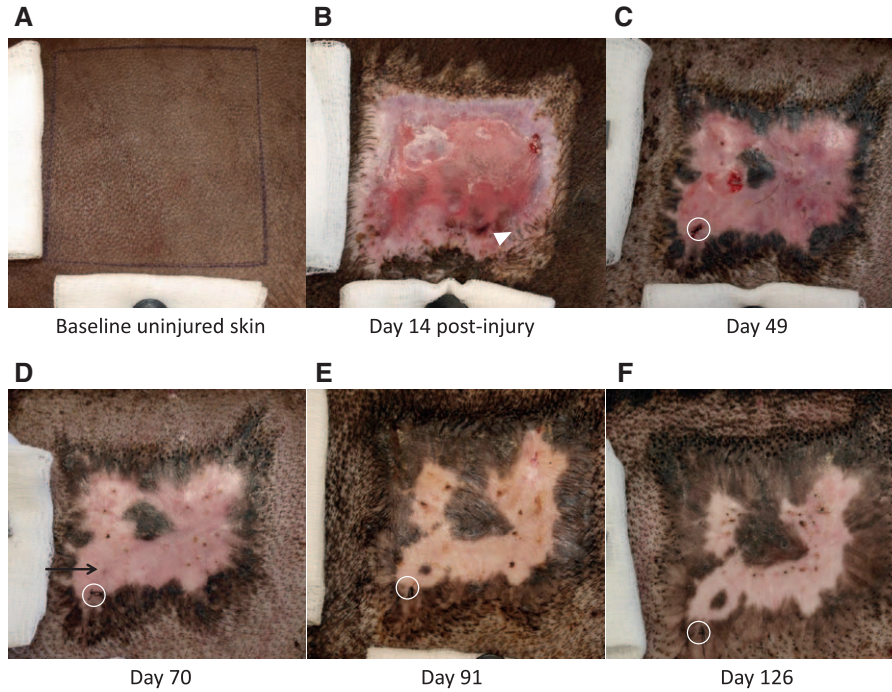

Figure 1. Macroscopic images of Duroc uninjured skin, wound, and scar. Images taken at a distance of 25 cm from the skin surface. A. Baseline uninjured skin. B. Wound 14 days postinjury with incomplete epithelialization. The arrowhead points to early hyperpigmented areas associated with surrounding uninjured skin and hair follicles. C. Day 49 after wound creation, early after completion of epithelialization. The circle indicates imaging reference suture. D. Day 70 after wound creation. The black arrow points to the first indication of a new island of hyperpigmented scar. The circle indicates imaging reference suture. E. Day 91 after wound creation. The circle indicates imaging reference suture. F. Day 126 after wound creation. The circle indicates imaging reference suture.

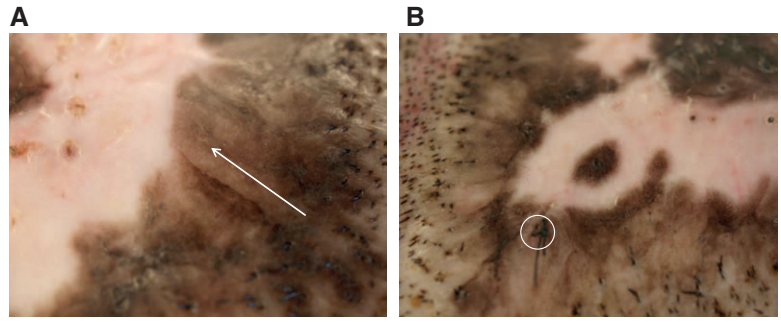

Figure 2. Magnified macroscopic images of Duroc hyperpigmented and hypopigmented scar. Peripheral areas of hyperpigmentation exhibited a pattern of expansion toward the center of the wound/scar, as seen in A, with the direction of expansion indicated by the arrow. Islands of hyperpigmented scar also arose that were completely surrounded by hypopigmented scar, as seen in B. These islands were not associated with hair follicles or normal, uninjured skin. The circle points out the reference suture used for spectral imaging.

encircled in Figures 1 and 2. One area of imaging included the hyperpigmented island seen in Figures 1D–F and 2B. As described, a minimization algorithm using melanin, oxygenated and deoxygenated hemoglobin, as well as water absorption coefficient data was used to reconstruct maps of melanin volume fraction, represented visually in Figure 3. This information was used to quantify melanin concentration within the imaged region of interest. The trend in melanin concentration within the region is represented graphically in Figure 4, with hyperpigmented and hypopigmented regions graphed over time, and the general volume fraction of melanin in normal uninjured skin represented for reference. Prior to approximately week 13 (day 91), the hyperpigmented region is analyzed to contain a melanin volume fraction less than that of normal uninjured skin, though it continued to increase in the following weeks. The data points for hyperpigmentation and hypopigmentation at week 18 correspond to the images seen in Figures 1F, 2B, and 3, which were also captured at week 18.

S100B is a known immunohistologic marker for melanocytes[20] and is also known to be absent in keratinocytes and fibroblasts.[21] Primary antibody to S100B was used to stain for melanocytes in hyperpigmented and hypopigmented tissue samples over the course of scar imaging and observation. An FITC-tagged anti-mouse secondary antibody was used to visualize stained cells by immunofluorescence. Both hyperpigmented and hypopigmented tissue samples contained S100B-positive melanocytes, at an average of 1 to 2 per ×400 imaging field. S100B-positive melanocytes in hyperpigmented skin can be visualized in Figure 5A, and S100B-positive melanocytes in hypopigmented skin can be visualized in Figure 5B. Positively stained cells were counted and revealed that there was no significant difference in the average

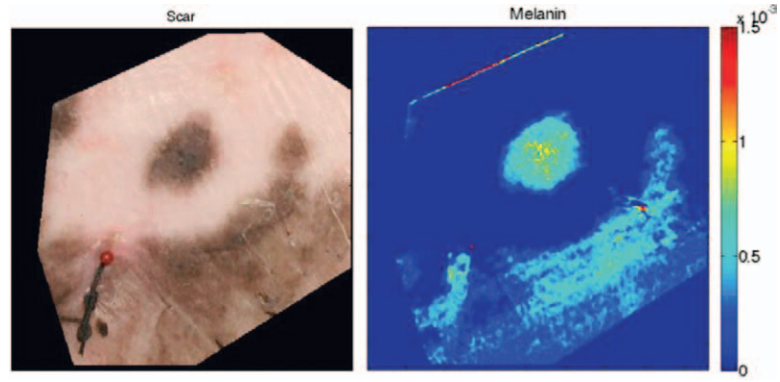

Figure 3. Photographic region of interest and melanin volume fraction map from spatial frequency domain imaging. Reference sutures were used to recreate the same imaging region of interest from week to week, seen in the left lower corner of both images. Dark blue in the melanin volume fraction map corresponds to a melanin volume fraction of zero. These images correspond to week 18 in Figure 4.

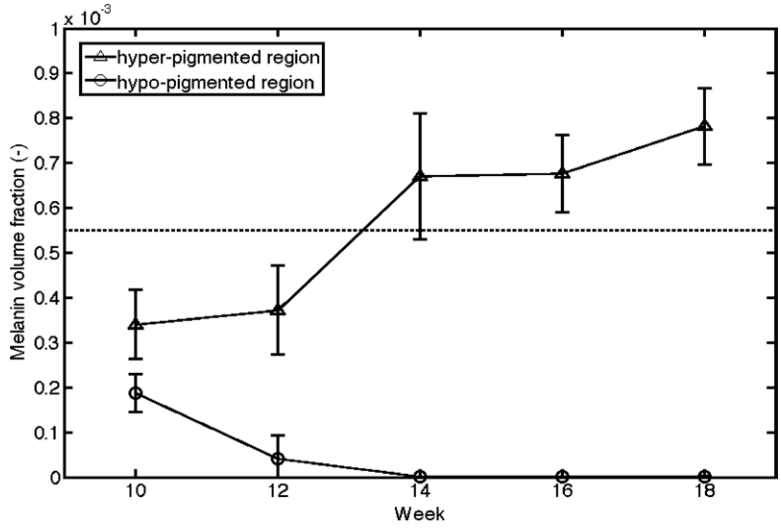

Figure 4. Graphical representation of melanin volume fraction maps created with spatial frequency domain imaging. The upper line with open triangles represents the melanin volume fraction of hyperpigmented areas within the region of interest. The lower line with open circles represents the melanin volume fraction of hypopigmented areas within the region of interest. The dashed line lies at the typical melanin volume fraction found in normal uninjured Duroc skin. Week 18 corresponds to the images shown in Figure 3.

number of melanocytes per 400× imaging field, as shown in Figure 6 ($P = .5203$, $n = 36$).

Azure B is a useful tool in evaluating melanocytic lesions immunohistochemically, as it counterstains melanin a green-blue color, allowing the brown chromogen of DAB to stand out from otherwise brown melanosomes.[22] Azure B stain was used to stain melanosomes green-blue for melanin quantification and for contrast with DAB-stained activated melanocytes. Consistent with spectral imaging, there was a clear increase in the amount of melanin staining of hyperpigmented scar as compared with both uninjured skin and hypopigmented scar (Figures 7C, A, and B, respectively). Uninjured skin also appeared to contain a greater amount of melanin than hypopigmented scar (Figure 7A vs B). Analysis of images quantifying Azure B staining showed that hyperpigmented scar sample images contained positive melanin staining over an average of $15.3 \pm 10.3\%$ of the imaged area, whereas uninjured skin and hypopigmented scar samples showed positive staining over $3.7 \pm 3.0\%$ and $2.0 \pm 2.2\%$ of the imaged areas, respectively (Figure 8). Hyperpigmented scars showed significantly greater staining than both hypopigmented scar and normal skin ($P < .0001$, $n = 68$). Interestingly, normal skin also showed significantly greater staining for melanin than hypopigmented scar ($P = .0043$, $n = 30$).

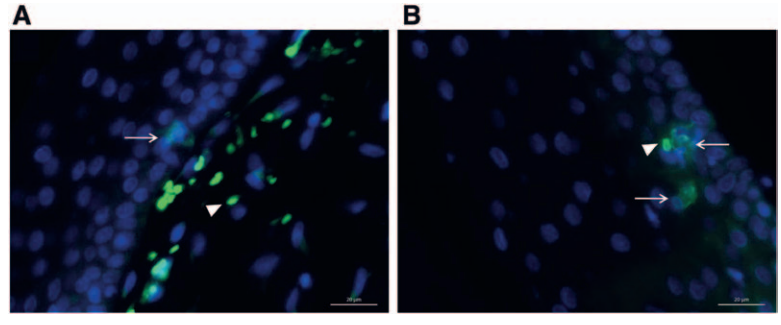

Figure 5. Representative immunofluorescent photomicrographs of S100B-stained hyperpigmented and hypopigmented scar samples. A florescein isothiocyanate-tagged anti-mouse secondary antibody was used to visualize stained cells by immunofluorescence. There was no difference in the average number of S100-positive cells between hyperpigmented and hypopigmented scar samples within a ×400 viewing field. Negative controls received secondary antibody only. 4',6-diamino-2-phenylindole-counterstained nuclei. Scale bar = 20 μm. ×400 magnification. A. Hyperpigmented scar. The arrow points to positively stained melanocytes. The arrowhead points to autofluorescent red blood cells. B. Hypopigmented scar. Arrows point to positively stained melanocytes. The arrowhead points to autofluorescent red blood cells.

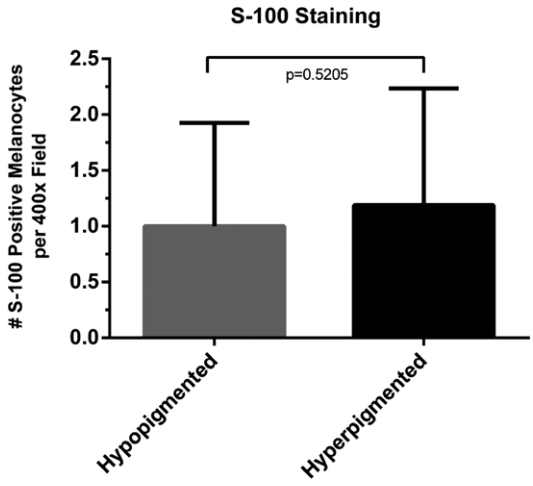

Figure 6. Hyperpigmented and hypopigmented scar samples were stained with primary antibody to S100B. A florescein isothiocyanate-tagged anti-mouse secondary antibody was used to visualize stained cells by immunofluorescence. There was no difference in the average number of S100-positive cells within a ×400 viewing field between hyperpigmented and hypopigmented scar samples. By a two-tailed unpaired Student's *t*-test, $P = .5205$, $n = 36$. Error bars represent SDs of the mean.

Primary antibody to HMB45 was used in combination with the Azure B staining above to identify active melanocytes, as it is known that in human tissue, HMB45 detects immature melanosomes in early-stage melanocytes and reactivated adult melanocytes, but does not stain normal adult epidermal melanocytes.[11,23] HMB45-positive melanocytes were identified in hyperpigmented scar at an average frequency of 1 to 2 per ×400 field of view, similar to that seen with S100B staining (Figure 7C). There were no HMB45-positive melanocytes identified in hypopigmented scar or normal uninjured skin. In some HMB45-stained melanocytes, dendritic projections toward neighboring keratinocytes could be visualized as well (Figure 7D).

α-MSH is known to bind the melanocortin 1 receptor (MC1R) leading to downstream expression of tyrosinase, required for the production of melanin.[24] To investigate melanocyte-stimulating activity, primary antibody to α-MSH was used in immunofluorescent staining of hyperpigmented and hypopigmented scar samples. A CY3-labeled anti-rabbit secondary antibody was used and cell nuclei were counterstained with DAPI (Figure 9). CY3 expression was measured and quantified relative to DAPI expression across samples. Hyperpigmented scar samples showed a greater average CY3 expression than hypopigmented samples (4.42 ± 3.60 vs 2.49 ± 2.53, $P = .0121$, $n = 42$) (Figure 10).

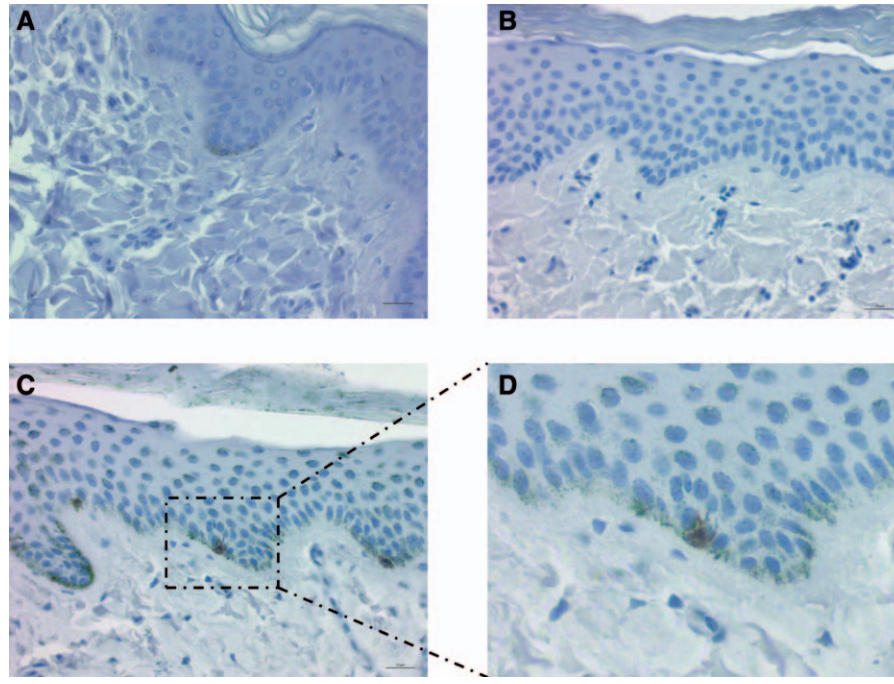

Figure 7. Representative photomicrographs of samples stained with Azure B and primary antibody to HMB45 with 3,3'-diaminobenzidine. Scale bar = 20 μm. A to C pictured at ×400 magnification. A. Uninjured Duroc skin showing some melanin staining at the base of the epidermis. No HMB45-positive melanocytes. B. Hypopigmented scar showing minimal melanin staining. No HMB45-positive melanocytes. C. Hyperpigmented scar showing widespread melanin staining from the basal layer of the epidermis up to the keratin layer. Occasional HMB45-positive melanocytes. Rectangle borders image enlarged in D. D. Enlarged portion of image C. HMB45-positive melanocytes with dendritic projections toward neighboring keratinocytes.

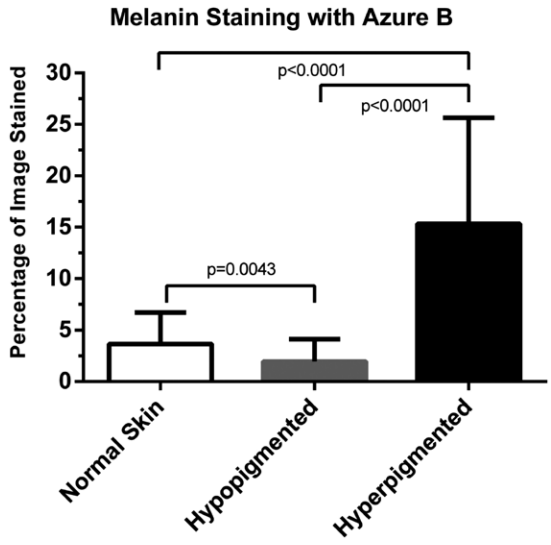

Figure 8. Azure B staining of melanin was quantified using Image J as a percentage of the imaged area positively stained. Normal skin showed an average of 3.7 ± 3.0%, hypopigmented scar showed an average of 2.0 ± 2.2%, and hyperpigmented scar showed an average of 15.3 ± 10.3%. Statistically significant differences were assessed using a two-tailed, unpaired Student's *t*-test, and are denoted by *P* values. $n = 30$ for uninjured skin samples, $n = 68$ for hyperpigmented samples, and $n = 53$ for hypopigmented samples. Error bars represent SDs of the mean.

DISCUSSION

Scars, especially hypertrophic scars, remain a challenging clinical issue. When scars are abnormally pigmented, they become even more distressing to patients and providers.[25] The continued investigation into hypertrophic scars and potential therapeutic targets should include the exploration of scar pigmentation and its pathophysiologic development.

It is well documented that melanocyte stem cells are located in the bulge region of hair follicles.[26] Melanocyte stem cells that transform into differentiated melanocytes have the capacity to form melanin when migrating to either hair bulbs or the surrounding epidermis.[4,26] Both epithelialization and pigmentation have previously been observed to increase radially from hair follicles, supporting the purported activity of these stem cells residing in the bulge area.[4,27] Melanocytes in association with hair follicles have additionally been implicated in various pigmentations of scar. The loss or destruction of hair follicles has been suggested as a cause of the common hypopigmentation seen in incisional epidermal scars,[26] while wound repigmentation studies consistently point to hair follicles as a source of melanocytes for restoring color to a reepithelialized wound.[25,28] The hypertrophic scars in the present study indeed appeared to have repigmentation associated spatially with normal uninjured skin and, consequently, hair follicles. The hypopigmented areas may potentially be explained, in part, by a lack of hair follicles present in the deep, large wounds created, and if these scars had been observed indefinitely, the pattern demonstrated in Figure 1 suggests that the entire scar may have eventually become hyperpigmented. The more perplexing components of the pigmentation patterns of these scars are two-fold: 1) the intensity of hyperpigmentation and 2) the isolated islands of hyperpigmentation observed. Even the hair-follicle-adjacent peripheries of these scars were not simply repigmented to a near-normal color; rather, they accumulated much darker pigmentation than preinjury, observed both grossly and microscopically with Azure B staining. Beyond this, the isolated islands of hyperpigmentation, which developed over time, were not associated with normal adjacent skin or hair

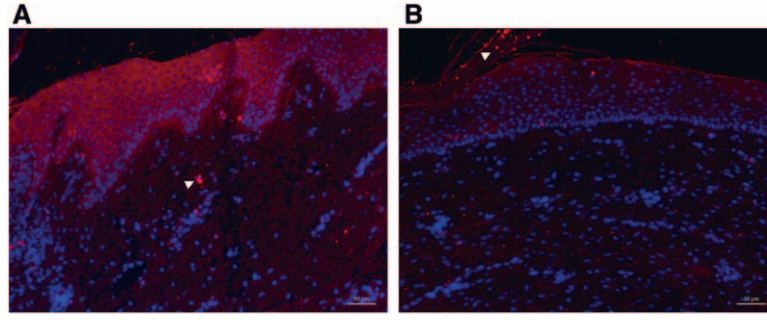

Figure 9. Representative immunofluorescent photomicrographs of α-melanocyte-stimulating hormone–stained hyperpigmented and hypopigmented scar samples. A CY3-tagged anti-rabbit secondary antibody was used to visualize stained cells by immunofluorescence. Hyperpigmented scars showed stronger staining for α-melanocyte-stimulating hormone on average than hypopigmented scars. Negative controls received secondary antibody only. 4',6-diamino-2-phenylindole-counterstained nuclei. Scale bar = 50 μm. ×100 magnification. A. Hyperpigmented scar. The arrowhead points to autofluorescent red blood cells. B. Hypopigmented scar. The arrowhead points to autofluorescent red blood cells.

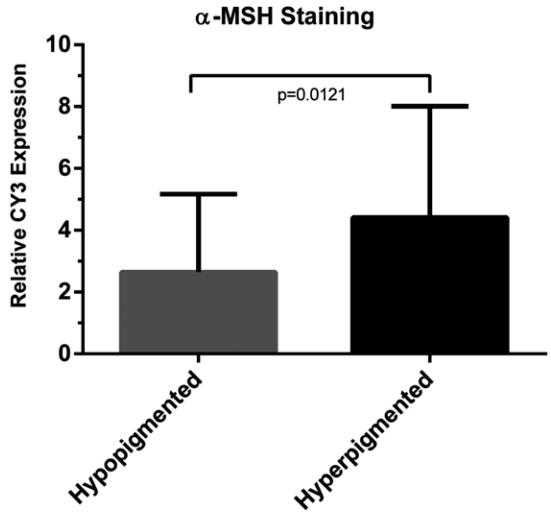

Figure 10. Immunofluorescent α-melanocyte-stimulating hormone (α-MSH) staining of scar samples was quantified using Zeiss Zen software. Relative CY3 expression as a function of DAPI expression is represented graphically. Hyperpigmented scar samples showed an average relative CY3 expression of 4.42 ± 3.60 and hypopigmented scar samples showed an average expression of 2.49 ± 2.53 ($P = .0121$, $n = 42$). Error bars represent SDs of the mean.

follicles, yet these darkened with the same intensity, and in some cases coalesced with the surrounding areas of hyperpigmentation. It is possible that the factors influencing the intensity of repigmentation to hyperpigmentation of the peripheries of these scars were also responsible for the more remote areas of hyperpigmentation.

The number of melanocytes between hyperpigmented and hypopigmented samples did not significantly differ in the current study, whereas the number of stimulated melanocytes, as evidenced by positive HMB45 staining, did. Those samples with positive HMB45-stained melanocytes also possessed large amounts of melanin, with clear evidence of melanosome transfer from melanocyte to keratinocyte and up superficially to the keratin layer of the skin (Figure 7C, D). Postinflammatory effects have been suggested by previous investigators as a potential mechanism for hyperpigmentation of scars, acting in similar ways to the hyperpigmentation seen after ultraviolet radiation damage of the skin, increasing the production of melanin and export of melanosomes to neighboring keratinocytes.[25] Additionally, stimulated melanocytes release a number of factors, many of which are important in inflammation; interleukin-1α (IL-1α), IL-2, IL-3, IL-6, IL-10, tumor necrosis factor-α, IL-8, chemokine ligand 2, TGF-β, catecholamines, eicosanoids, serotonin, nitric oxide, and α-MSH are among the many products of melanocytes.[6,29] Some of these secretion factors act in an autocrine fashion, with melanocyte inhibition occurring via IL-1, IL-6, and TNF-α, but stimulation via eicosanoids and α-MSH.[6,30] α-MSH acts on MC1R, which activates micropthalmia-associated transcription factor, leading to the expression of tyrosinase, a necessary enzyme for melanin production.[24] Activation of the MC1R/α-MSH signaling pathway has been associated with regulation of both inflammation and the extracellular matrix environment.[9] α-MSH itself has been described as anti-inflammatory, downregulating the production of IL-1, IL-4, IL-6, interferon-γ, and TNF-α,[31] while increasing the production of IL-10,[9,32,33] adding further complexity to the feedback loops that appear to exist between melanocytes, their products, and the inflammatory processes inherent to wound healing.

Inflammation was certainly a contributing factor in this swine model, simply by the nature of healing a large, full-thickness wound and the resultant fibroproliferative processes. α-MSH was found to be increased in those areas of scar that were hyperpigmented compared with those that were hypopigmented; however, it is unlikely that this one factor alone explains not only the intensity of hyperpigmentation seen, but the curious pattern of its appearance as well. Evidence exists that α-MSH possesses some activities independent of MC1R and reduces TGF-β1-induced synthesis of collagens I and III in fibroblasts.[9,34] The continued effort to understand the myriad of actors in the processes of inflammation, wound healing, fibrosis, and scar formation should likely include additional questions about α-MSH and special attention to the problems of both hyperpigmentation and hypopigmentation, as these appear to not be simply explained by hair follicle proximity.

Finally, the current study of the characteristics of abnormally pigmented hypertrophic scars used a spectral imaging system whose data output correlated with the observed macroscopic and microscopic appearances of scars. Furthermore, this unique imaging modality provided a method for estimating melanin concentration noninvasively. The continued use of this tool in concert with further elucidation of the characteristics of dyspigmented scar may allow for future predictive capabilities and therapeutic interventions prior to clinically apparent abnormal skin pigmentation.

CONCLUSIONS

In a red Duroc model of human scar formation, melanocyte quantity does not appear to influence

pigmentation, whereas the production of melanin does correlate with the pigmented appearances of skin and scars. Hyperpigmented scars appear to contain activated melanocytes, as evidenced by HMB45 staining, and increased levels of α-MSH. These observations open the door to investigating melanocyte stimulation and the inflammatory environment within a wound that may influence melanocyte activity. SFDI can be used to identify areas of melanin content in mature, pigmented scars, which may lead to its usefulness in wounds at earlier time points before markedly apparent pigmentation abnormalities.

REFERENCES

1. Tyack ZF, Pegg S, Ziviani J. Postburn dyspigmentation: its assessment, management, and relationship to scarring—a review of the literature. J Burn Care Rehabil 1997;18:435–40.
2. Wisely JA, Hoyle E, Tarrier N, Edwards J. Where to start? Attempting to meet the psychological needs of burned patients. Burns 2007;33:736–46.
3. Zeitlin RE. Long-term psychosocial sequelae of paediatric burns. Burns 1997;23:467–72.
4. Lin JY, Fisher DE. Melanocyte biology and skin pigmentation. Nature 2007;445:843–50.
5. Velangi SS, Rees JL. Why are scars pale? An immunohistochemical study indicating preservation of melanocyte number and function in surgical scars. Acta Derm Venereol 2001;81:326–8.
6. Cichorek M, Wachulska M, Stasiewicz A, Tymińska A. Skin melanocytes: biology and development. Postepy Dermatol Alergol 2013;30:30–41.
7. Fitzpatrick TB, Breathnach AS. The epidermal melanin unit system. Dermatol Wochenschr 1963;147:481–9.
8. Gao FL, Jin R, Zhang L, Zhang YG. The contribution of melanocytes to pathological scar formation during wound healing. Int J Clin Exp Med 2013;6:609–13.
9. Muffley LA, Zhu KQ, Engrav LH, Gibran NS, Hocking AM. Spatial and temporal localization of the melanocortin 1 receptor and its ligand α-melanocyte-stimulating hormone during cutaneous wound repair. J Histochem Cytochem 2011;59:278–88.
10. Sullivan TP, Eaglstein WH, Davis SC, Mertz P. The pig as a model for human wound healing. Wound Repair Regen 2001;9:66–76.
11. Chadwick SL, Yip C, Ferguson MW, Shah M. Repigmentation of cutaneous scars depends on original wound type. J Anat 2013;223:74–82.
12. Gallant-Behm CL, Olson ME, Hart DA. Cytokine and growth factor mRNA expression patterns associated with the hypercontracted, hyperpigmented healing phenotype of red duroc pigs: a model of abnormal human scar development? J Cutan Med Surg 2005;9:165–77.
13. Travis T, Mino, MJ, Mauskar, NA, Jo, DY, Ghassemi, P, Moffatt, LT, Jordan, MH, Ramella-Roman, JC, Shupp, JW. A novel and reproducible porcine scar model for testing the effects of pressure therapy while correlating non-invasive imaging metrics to molecular and histological changes 45th Annual Meeting of the American Burn Association; Palm Springs, CA; 2013.
14. Mino MJ, Mauskar NA, Matt SE, et al. A fitted neoprene garment to cover dressings in swine models. Lab Anim (NY) 2012;42:23–5.
15. Ghassemi P, Shupp, JW, Moffatt, LT, Ramella-Roman, JC. A novel spectral imaging system for quantitative analysis of hypertrophic scar. ProcSPIE; 2013.
16. Ghassemi P, Travis, TE, Shupp, JW, Moffatt, LT, Ramella-Roman, JC. Monitoring the influence of compression therapy on pathophysiology and structure of a swine scar model using a multispectral imaging system. Proc SPIE; 2014.
17. Nguyen TT, Ramella-Roman JC, Moffatt LT, Ortiz RT, Jordan MH, Shupp JW. Novel application of a spatial frequency domain imaging system to determine signature spectral differences between infected and noninfected burn wounds. J Burn Care Res 2013;34:44–50.
18. Hale GM, Brown RE, Jarmie N. Pole structure of the J pi =3/2(+) resonance in 5He. Phys Rev Lett 1987;59:763–6.
19. Takatani H, Oka M, Fukuda M, et al. Gene mutation analysis and quantitation of DNA topoisomerase I in previously untreated non-small cell lung carcinomas. Jpn J Cancer Res 1997;88:160–5.
20. Shrestha P, Muramatsu Y, Kudeken W, et al. Localization of Ca(2+)-binding S100 proteins in epithelial tumours of the skin. Virchows Arch 1998;432:53–9.
21. Cheong KA, Noh M, Kim CH, Lee AY. S100B as a potential biomarker for the detection of cytotoxicity of melanocytes. Exp Dermatol 2014;23:165–71.
22. Kamino H, Tam ST. Immunoperoxidase technique modified by counterstain with azure B as a diagnostic aid in evaluating heavily pigmented melanocytic neoplasms. J Cutan Pathol 1991;18:436–9.
23. Smoller BR, Hsu A, Krueger J. HMB-45 monoclonal antibody recognizes an inducible and reversible melanocyte cytoplasmic protein. J Cutan Pathol 1991;18:315–22.
24. Wen KC, Chang CS, Chien YC, et al. Tyrosol and its analogues inhibit alpha-melanocyte-stimulating hormone induced melanogenesis. Int J Mol Sci 2013;14:23420–40.
25. Chadwick S, Heath R, Shah M. Abnormal pigmentation within cutaneous scars: a complication of wound healing. Indian J Plast Surg 2012;45:403–11.
26. Gola M, Czajkowski R, Bajek A, Dura A, Drewa T. Melanocyte stem cells: biology and current aspects. Med Sci Monit 2012;18:RA155–9.
27. Ansell DM, Kloepper JE, Thomason HA, Paus R, Hardman MJ. Exploring the "hair growth-wound healing connection": anagen phase promotes wound re-epithelialization. J Invest Dermatol 2011;131:518–28.
28. SNELL RS. A study of the melanocytes and melanin in a healing deep wound. J Anat 1963;97:243–53.
29. Lu Y, Zhu WY, Tan C, Yu GH, Gu JX. Melanocytes are potential immunocompetent cells: evidence from recognition of immunological characteristics of cultured human melanocytes. Pigment Cell Res 2002;15:454–60.
30. Slominski A, Tobin DJ, Shibahara S, Wortsman J. Melanin pigmentation in mammalian skin and its hormonal regulation. Physiol Rev 2004;84:1155–228.
31. Brzoska T, Luger TA, Maaser C, Abels C, Böhm M. Alpha-melanocyte-stimulating hormone and related tripeptides: biochemistry, antiinflammatory and protective effects in vitro and in vivo, and future perspectives for the treatment of immune-mediated inflammatory diseases. Endocr Rev 2008;29:581–602.
32. Bhardwaj RS, Schwarz A, Becher E, et al. Pro-opiomelanocortin-derived peptides induce IL-10 production in human monocytes. J Immunol 1996;156:2517–21.
33. Redondo P, García-Foncillas J, Okroujnov I, Bandrés E. Alpha-MSH regulates interleukin-10 expression by human keratinocytes. Arch Dermatol Res 1998;290:425–8.
34. Böhm M, Raghunath M, Sunderkötter C, et al. Collagen metabolism is a novel target of the neuropeptide alpha-melanocyte-stimulating hormone. J Biol Chem 2004;279:6959–66.